Stability Analysis of Micropipette Aspiration of Neutrophils

Jure Derganc,* Bojan Božič,* Saša Svetina,*† and Boštjan Žekš*†
*Institute of Biophysics, Medical Faculty, University of Ljubljana, Lipičeva 2, SI-1000 Ljubljana and †J. Stefan Institute, Jamova 39, SI-1111 Ljubljana, Slovenia

ABSTRACT During micropipette aspiration, neutrophil leukocytes exhibit a liquid-drop behavior, i.e., if a neutrophil is aspirated by a pressure larger than a certain threshold pressure, it flows continuously into the pipette. The point of the largest aspiration pressure at which the neutrophil can still be held in a stable equilibrium is called the critical point of aspiration. Here, we present a theoretical analysis of the equilibrium behavior and stability of a neutrophil during micropipette aspiration with the aim to rigorously characterize the critical point. We take the energy minimization approach, in which the critical point is well defined as the point of the stability breakdown. We use the basic liquid-drop model of neutrophil rheology extended by considering also the neutrophil elastic area expansivity. Our analysis predicts that the behavior at large pipette radii or small elastic area expansivity is close to the one predicted by the basic liquid-drop model, where the critical point is attained slightly before the projection length reaches the pipette radius. The effect of elastic area expansivity is qualitatively different at smaller pipette radii, where our analysis predicts that the critical point is attained at the projection lengths that may significantly exceed the pipette radius.

INTRODUCTION

Micropipette aspiration is an important experimental method in the research of the rheology of resting neutrophil leukocytes. In this experiment, one studies the behavior of a single neutrophil as it is controllably aspirated into a micropipette narrower than its diameter. A commonly observed behavior of neutrophils during the micropipette experiment is the following (Evans and Kukan, 1984): In the free state, a resting neutrophil is spherical. If a small aspiration pressure is applied, the neutrophil projects into the pipette and attains an equilibrium. In contrast, if the applied aspiration pressure is above a certain threshold, the so-called critical pressure, the neutrophil does not reach an equilibrium but flows continuously into the pipette. Finally, if the neutrophil is released from the pipette, it recovers its initial spherical shape.

Evans and Kukan (1984) were the first to recognize that this behavior can be explained by a liquid-drop nature of neutrophils. They introduced the now generally accepted liquid-drop model of neutrophil viscoelasticity, in which the neutrophil is regarded as a Newtonian fluid drop with a constant surface tension. The neutrophil surface tension has been related to the neutrophil membrane cortex (Evans and Kukan, 1984), therefore it is usually denoted as the *cortical tension*. A general discussion on the validity of the basic liquid-drop model and a good basis for further research of dynamics of micropipette aspiration was given recently by Drury and Dembo (1999).

Received for publication 20 July 1999 and in final form 14 March 2000.

Address reprint requests to Mr. Jure Derganc, Institute of Biophysics, Medical Faculty, Lipiceva 2, SI-1105 Ljubljana, Slovenia. Tel.: +386-61-314-127; Fax: +386-61-13-15-127; E-mail: jure.derganc@biofiz.mf.uni-lj.si.

0006-3495/00/07/153/10 $2.00

Evans and Yeung (1989) recognized that the liquid-drop model alone could not explain all neutrophil features and that the neutrophil could exhibit also some elastic behavior, as had been proposed in an earlier study by Schmid-Schönbein et al. (1981). Many attempts were made to combine the liquid and the elastic nature of neutrophils. Some of the extended models attributed elasticity to the whole neutrophil (Dong and Skalak, 1992), whereas others focused more on the elasticity of the membrane cortex. For example, the existence of a nonconstant cortical tension was investigated (Needham and Hochmuth, 1992), and the importance of cortex bending rigidity was examined (Zhelev et al., 1994). However, it has not been shown that any of these refined models completely describes both the dynamic (i.e., the continuous flow) and the static equilibrium behavior of neutrophils.

The micropipette experiment has also been used in the research of the possible underlying molecular mechanisms that govern neutrophil mechanical properties. For example, research was carried out to establish the dependence of neutrophil mechanical rigidity on the polymerization rate of its actin filaments (Tsai et al., 1994) and microtubules (Tsai et al., 1998). Because these experiments rely on the quantitative measurements of the neutrophil viscoelastic parameters, a good theoretical characterization of these parameters is of great importance. One of the neutrophil viscoelastic parameters, its cortical tension, is normally determined by measuring the critical aspiration pressure. However, the notion of the critical pressure in the literature is ambiguous. It is usually based on the prediction of the basic liquid-drop model and the approximation that the critical pressure is attained when the neutrophil projection length in the pipette reaches the pipette radius (Yeung and Evans, 1989). This supposition should be applied carefully, though. Because the critical pressure is the maximal possible aspiration pressure at which the cell can still be held in a static equilibrium,

the equilibrium projection lengths longer than the pipette radius are unstable and should not be observed. However, in fact, it seems that the stable equilibrium of the aspirated neutrophil could be observed even for projection lengths much larger than the pipette radius (Evans and Yeung, 1989; Zhelev and Hochmuth, 1994). Although such behavior cannot be explained within the basic liquid-drop model, it can be intuitively expected as a consequence of neutrophil elasticity.

In this paper, we present a theoretical analysis of the critical aspiration pressure behavior, based on the basic liquid-drop model extended by also considering neutrophil elasticity. Specifically, we are taking into account the nonconstant cortical tension as it was observed by Needham and Hochmuth (1992). Accordingly, the neutrophil is considered as a liquid drop with an apparent elastic area expansivity modulus. We focus on the equilibrium behavior of the aspirated neutrophil and its stability. In this way, the critical aspiration pressure can be identified as the aspiration pressure at which stability of the aspirated neutrophil breaks and the neutrophil starts to flow into the pipette. Consequently, the point of the stability breakdown, i.e., the critical point of aspiration, can be well characterized and the corresponding values of the critical aspiration pressure and the critical projection length can be calculated. Our analysis provides the predictions for the critical projection length and the critical aspiration pressure and can therefore be used to better evaluate the measurements of the neutrophil cortical tension. In addition, the analysis can serve as a basis for further measurements of the apparent neutrophil elastic area expansivity modulus. The paper is organized as follows. We will first discuss the significant terms of neutrophil energy that govern neutrophil equilibrium behavior. Then we will apply the variational approach to calculate the equilibrium states of the aspirated neutrophil and determine stability of these equilibrium states. Finally, we will present the predictions for the position of the critical point of aspiration.

THEORY

Model: liquid droplet with an elastic surface

To understand the limitations of neutrophil mechanical properties models, one should bear in mind the complex structure of neutrophils. Free resting neutrophils are wrinkled spherical cells of ~ 8 μm in diameter (Bessis, 1973; Ting-Beall et al., 1993). When a neutrophil is deformed from the spherical shape, the wrinkles are smoothing out and the apparent neutrophil area enlarges. The wrinkles provide enough material for extensions up to approximately two times the initial spherical area (Evans and Yeung, 1989). The investigation of the neutrophil interior structure reveals many small granules and the cell nucleus floating in the neutrophil cytoplasm. These organelles were estimated to comprise around 37% of the total cell volume (Schmid-Schönbein et al., 1980). Another important neutrophil structure is the membrane cortex, which supports the outer plasma membrane. It is composed mainly of actin filaments meshwork and has an approximate thickness of $0.1-0.2$ μm (Sheterline and Rickard, 1989; Zhelev et al., 1994).

The analysis in the present paper is based on the basic liquid-drop model extended by including the neutrophil elastic area expansivity. The neutrophil is thus considered as an incompressible homogeneous fluid with a cortical tension, which increases with the apparent neutrophil surface area dilation (Needham and Hochmuth, 1992). Within this model, the equilibrium behavior of an aspirated neutrophil is governed exclusively by its *cortical energy*, i.e., the energy of its membrane-cortex complex. In a general case, this might be an oversimplification, but as long as the deformations are not too large and the organelles do not touch the membrane, and because we are focusing only on the equilibrium states of aspiration, this assumption is justified. In addition, during the normal course of micropipette aspiration, the adhesion of resting neutrophils to the pipette glass is negligible (Evans and Kukan, 1984; Needham and Hochmuth, 1992) and can be, therefore, safely omitted from the analysis. Also, in our model, we do not consider the bending rigidity of the cortex, which may become important in the case of aspiration into very narrow pipettes (Zhelev et al., 1994).

The exact microscopical origin of the cortical tension is not known, however, evidences exist that it is related to the actin filaments in the cortex (Tsai et al., 1994; Tsai et al., 1998). For example, the tension could be a consequence of some active processes, which constantly drive the actin filaments one across another and contract the cortex. Another imaginable origin of one part of the constant cortical tension could be attributed to a possible difference of the surface energy of the lipid bilayer stocked in the wrinkles and the bilayer stretched on the actin cortex (Svetina et al., 1998)—if the bilayer preferred to reside in the wrinkles, the result would be a contractile cortical tension. Needham and Hochmuth (1992) indicated that the cortical tension might change with the activation of the neutrophil.

Because the exact physical origin of the tension is not known, the cortical energy has to be described phenomenologically. To include the nonconstant cortical tension, the cortical energy is expanded up to the second power in the neutrophil area,

$$W = \gamma A + \frac{1}{2}\frac{K}{A_0}(A - A_0)^2, \tag{1}$$

where γ is the constant part of the cortical tension, A is the neutrophil area, K is the area expansivity modulus, and A_0 is taken to be the area of the free spherical neutrophil. The value of A_0 is fixed with the neutrophil volume V_0, which is constant during a typical aspiration under stable osmotic

conditions. The quadratic term in Eq. 1 can be interpreted as the neutrophil elastic area expansivity term. Indications exist that the parameters γ and K may depend on the history of aspiration, i.e., the increase of the rate of actin polymerization in the cortex may be induced by the applied stress (Zhelev and Hochmuth, 1994).

The effective cortical tension associated with the cortical energy defined above is

$$\bar{T} = \frac{\partial W}{\partial A} = \gamma + K\frac{A - A_0}{A_0}. \tag{2}$$

For positive constants γ and K, the cortical tension is also positive and thus tends to minimize the cell area. When the neutrophil is undeformed, $A = A_0$, the cortical tension has the value of γ. This definition of the parameters K and γ is consistent with the one proposed by Needham and Hochmuth (1992).

To emphasize that our analysis applies to very idealized neutrophils, we will use the term "elastic droplet" when referring to the neutrophil within the extended liquid drop model, and "liquid droplet" when referring to the basic liquid-drop model.

Equilibrium states

Thermodynamically, the equilibrium of an aspirated droplet is characterized as the state of the extreme thermodynamic potential of the system. Within the presented model of micropipette aspiration, the work done by aspiration is entirely transformed into cortical energy, and the thermodynamic potential of an aspirated droplet can be written as

$$G = -\Delta P V_p + \gamma A + \frac{1}{2}\frac{K}{A_0}(A - A_0)^2, \tag{3}$$

where ΔP is the aspiration pressure and V_p is the droplet volume aspirated into the pipette. The aspiration pressure, ΔP, is defined as the difference between the pressure of the solution outside the pipette and the pressure in the pipette and is positive during aspiration.

The extrema of the thermodynamic potential defined in Eq. 3 can be found by means of the calculus of variations. The extrema (i.e., the equilibrium states of an aspirated droplet) are the states where the variation of the thermodynamic potential with respect to all variables and to the shape of the droplet is zero, $\delta G = 0$. It turns out that the equilibrium shapes of an elastic droplet are the same as in the case of a liquid droplet. This can be seen from the fact that the variation of the potential δG can be written in the same form as in the basic liquid drop model:

$$\begin{aligned}\delta G &= -\Delta P \delta V_p + \gamma \delta A + K\left(\frac{A}{A_0} - 1\right)\delta A \\ &= -\Delta P \delta V_p + \bar{T}\delta A.\end{aligned} \tag{4}$$

The variation of G depends on the effective cortical tension. The variational procedure sees no difference between the constant tension and the effective one, because, in both cases, the tension is just a parameter of a given equilibrium state. Therefore, the equilibrium states of an elastic droplet are exactly the same as the equilibrium states of a liquid droplet.

Thus, two general results concerning the equilibrium states of a liquid droplet, widely used in the literature, are valid also in the case of an elastic droplet (the full derivation of these results is given in the Appendix A):

1. The equilibrium shapes of an aspirated droplet are composed of spherical and cylindrical parts (Fig. 1). The free droplet is a sphere with the radius R_0. As aspiration proceeds, the droplet projection in the pipette grows, the radius of the spherical part in the pipette R_{in} decreases and the projection length L_p increases. When R_{in} (and L_p) reaches the pipette radius R_p, the projection continues to grow as a cylinder with a hemispherical cap of the same radius as the pipette. The radius of the spherical part of the droplet outside the pipette is denoted by R_{out}.
2. The equilibrium aspiration pressure is related to the cortical tension by the law of Laplace,

$$\Delta P = 2\bar{T}\left(\frac{1}{R_{in}} - \frac{1}{R_{out}}\right), \tag{5}$$

where $\bar{T}$ is the effective cortical tension given by Eq. 2.

Because of the simple geometry of the equilibrium states, the overall droplet equilibrium shape is fully defined by only two geometrical variables, the radius R_{out} and the projection length L_p. In terms of these two variables, the

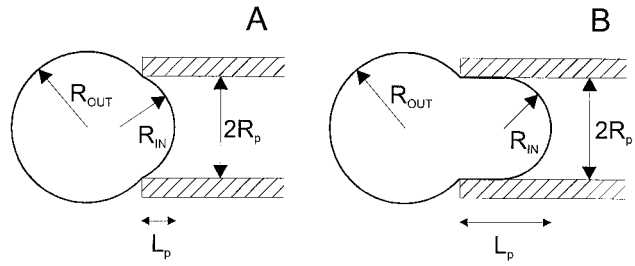

FIGURE 1 Schematic representation of the droplet equilibrium shape during aspiration into a micropipette. (*A*) The projection length is less than the pipette radius and the shape is composed of two spherical parts; (*B*) The projection length exceeds the pipette radius and the projection is composed of a cylinder with a hemispherical cap of the same radius as the pipette. The radius of the outer spherical part is R_{out}, the radius of the part in the pipette is R_{in}, the droplet projection length in the pipette is L_p, and the radius of the pipette is R_p. Note that, if $L_p \geq R_p$, the value of R_{in} equals the pipette radius, $R_{in} = R_p$.

equilibrium area and volume of a droplet are expressed as

$$A = \begin{cases} 2\pi R_{out}(R_{out} + \sqrt{R_{out}^2 - R_p^2}) + \pi(2R_p^2 + L_p^2) \\ \qquad\qquad \text{if} \quad L_p < R_p \\ 2\pi R_{out}(R_{out} + \sqrt{R_{out}^2 - R_p^2}) + 2\pi R_p L_p \\ \qquad\qquad \text{if} \quad L_p > R_p, \end{cases} \tag{6}$$

$$V = \begin{cases} \frac{2}{3}\pi R_{out}^3 + \frac{1}{3}\pi(2R_{out}^2 + R_p^2)\sqrt{R_{out}^2 - R_p^2} \\ \quad + \frac{1}{6}\pi L_p(3R_p^2 + L_p^2) \quad \text{if } L_p < R_p \\ \frac{2}{3}\pi R_{out}^3 + \frac{1}{3}\pi(2R_{out}^2 + R_p^2)\sqrt{R_{out}^2 - R_p^2} \\ \quad + \pi R_p^2 L_p - \frac{1}{3}\pi R_p^3 \quad \text{if } L_p > R_p. \end{cases} \tag{7}$$

Furthermore, because the volume of the droplet during aspiration is constant, R_{out} and L_p are connected by the constant volume constraint $V = V_0$. Therefore, only one geometrical variable is truly independent, and the entire set of the equilibrium shapes can be obtained and examined by varying only one geometrical variable. The computational procedure to calculate the equilibrium states used in our analysis was the following: for a given value of R_p and R_{out}, the constant volume constraint was used to calculate the corresponding L_p. The corresponding value of R_{in} was obtained from the geometrical relations connecting R_{in} and L_p:

$$R_{in} = \begin{cases} \frac{1}{2}(L_p^2 + R_p^2)/L_p & \text{if } L_p < R_p \\ R_p & \text{if } L_p > R_p. \end{cases} \tag{8}$$

Then, the equilibrium aspiration pressure was determined by using the law of Laplace (Eq. 5). Finally, Eq. 3 was applied to calculate the corresponding thermodynamic potential. At a given pipette radius, the whole set of the possible equilibrium states was obtained by varying R_{out} from $R_{out} = R_0$ (which corresponds to the free spherical droplet at zero aspiration pressure, $\Delta P = 0$) to $R_{out} = R_p$ (the droplet is aspirated completely to a cigar shape and the corresponding equilibrium aspiration pressure is again zero, $\Delta P = 0$).

The radius R_{in} is a smooth function of the projection length L_p. However, because there are two distinct regimes of the projection growth in the pipette, the function $R_{in}(L_p)$ has a discontinuous second derivative in the point where L_p reaches R_p. As a consequence, the same is true also for the equilibrium aspiration pressure $\Delta P(L_p)$.

Introduction of the relative dimensionless quantities

Because the choice of the scale within the presented model does not affect the behavior of the system, the analysis can be simplified by the normalization of the involved quantities. The natural way to normalize these quantities is to introduce relative dimensionless quantities that have been scaled by the initial spherical size of the droplet and the constant part of the cortical tension γ. These relative dimensionless quantities will be written in lowercase. The radii and the projection length are normalized relative to the radius of the initial sphere ($r_p = R_p/R_0$, $r_{in} = R_{in}/R_0$, $r_{out} = R_{out}/R_0$, and $l_p = L_p/R_0$), the areas relative to the initial droplet area ($a = A/A_0$, and $a_0 = 1$), and the volume relative to the constant droplet volume ($v_p = V_p/V_0$). In the dimensionless form, all possible ratios between the pipette radius and the neutrophil radius are obtained by varying the relative pipette radius r_p from 0 to 1.

The relative thermodynamic potential and relative aspiration pressure are

$$g = \frac{G}{\gamma A_0}, \quad (\gamma A_0 \approx 6 \times 10^{-15}\ \text{J} \approx 1 \times 10^6\ \text{kT}), \tag{9}$$

$$\Delta p = \frac{\Delta P V_0}{\gamma A_0}, \quad \left(\frac{\gamma A_0}{V_0} \approx 23\ \text{Pa}\right). \tag{10}$$

The values in the parentheses represent typical energy and pressure scales from the experiments. They are obtained by using a typical neutrophil size (with $R_0 = 4\ \mu$m) and a typical value of the cortical tension $\gamma = 30\ \mu$N/m; the measured values of γ lie in the range from 24 μN/m (Needham and Hochmuth, 1992) to 35 μN/m (Evans and Yeung, 1989).

Using the relative dimensionless quantities, the thermodynamic potential is written as

$$g = -\Delta p v_p + a + \frac{1}{2}\frac{K}{\gamma}(a - 1)^2. \tag{11}$$

Note that the only parameter of the system material properties is the ratio between the area expansivity modulus and the constant part of the cortical tension K/γ. The basic liquid-drop model is obtained if this parameter is set to zero ($K/\gamma = 0$), whereas the measured value of the ratio is on the order of unity ($K/\gamma \sim 1$), (Needham and Hochmuth, 1992).

Stability of equilibrium states

Not all the equilibrium states of an aspirated droplet calculated by the procedure described above are in a stable equilibrium. Thermodynamically, the stable equilibrium states are only the states of the minimal thermodynamic potential, whereas the states of the maximal thermodynamic potential are in an unstable equilibrium. If a state was in an unstable equilibrium, a small fluctuation would drag it away to a nearby stable equilibrium.

By choosing the relative projection length l_p as the only free geometrical variable of the equilibrium states, the stability condition for the equilibrium states of an aspirated

droplet can be mathematically expressed as

$$\frac{d^2g}{dl_p^2} > 0. \quad (12)$$

It is possible and useful to translate this stability condition into a condition connecting the observable quantities Δp and l_p. The stability condition can be thus written as (for a detailed derivation see Appendix B)

$$\frac{d\Delta p}{dl_p} > 0. \quad (13)$$

Intuitively, this is a reasonable condition, analogous to the fact that the bulk modulus in the standard thermodynamics is always positive. If, for an equilibrium state, one needed to decrease the aspiration pressure to increase the projection length, such a state would be unstable.

RESULTS

Critical point

The critical point of micropipette aspiration can be characterized as the point of the equilibrium state's stability breakdown. It can be analyzed by considering the relation between the equilibrium aspiration pressure Δp and the corresponding projection length l_p (via the law of Laplace, Eq. 5), and by using the stability condition (Eq. 13). The dependence of the equilibrium projection length on the aspiration pressure during a typical course of aspiration is presented in Fig. 2. At the beginning of aspiration, the projection length increases with increasing aspiration pressure. These states are in a stable equilibrium because the derivative $d\Delta p/dl_p$ is positive. The point where the equilibrium aspiration pressure reaches its maximum (i.e., where $d\Delta p/dl_p = 0$) is the critical point of aspiration. The corresponding aspiration pressure and projection length are the critical aspiration pressure Δp_{crit} and the critical projection length $l_{p(crit)}$. If the pressure is increased above the critical pressure, the droplet starts to flow continuously into the pipette and therefore enters the dynamic regime, which is not covered by our analysis. The equilibrium states, with projection lengths exceeding the critical projection length, have a negative $d\Delta p/dl_p$ and are in an unstable equilibrium.

As can be seen from Fig. 2, the elasticity of the droplet strongly affects the position of the critical point. For small ratios K/γ, the critical projection length is near the pipette radius, but it can increase significantly with higher K/γ. Note that, in the case of $K/\gamma = 1$ and $r_p = 0.5$ (*curve c* in Fig. 2), only a small aspiration pressure difference is needed to aspirate the droplet from $l_p = r_p$ to the critical projection length $l_p = l_{p(crit)} \approx 3r_p$.

The stability of the equilibrium states can be examined further by considering the values of the equilibrium thermodynamic potential (Eq. 11). As expected, the unstable equilibrium states are at a higher thermodynamic potential than the stable equilibrium states (Fig. 3). A droplet in an unstable equilibrium state would either slightly withdraw from the pipette and reach the stable equilibrium state at the same pressure or enter the continuous flow regime. Furthermore, because of the fluctuations, spontaneous transitions from a stable equilibrium state (over the maximum pertaining to the unstable equilibrium states) to the dynamic regime at a fixed pressure could be theoretically possible before the critical point. However, the energy barrier to be overcome is several orders of magnitude larger than the thermal energy kT (compare the energy scale in Fig. 3 and

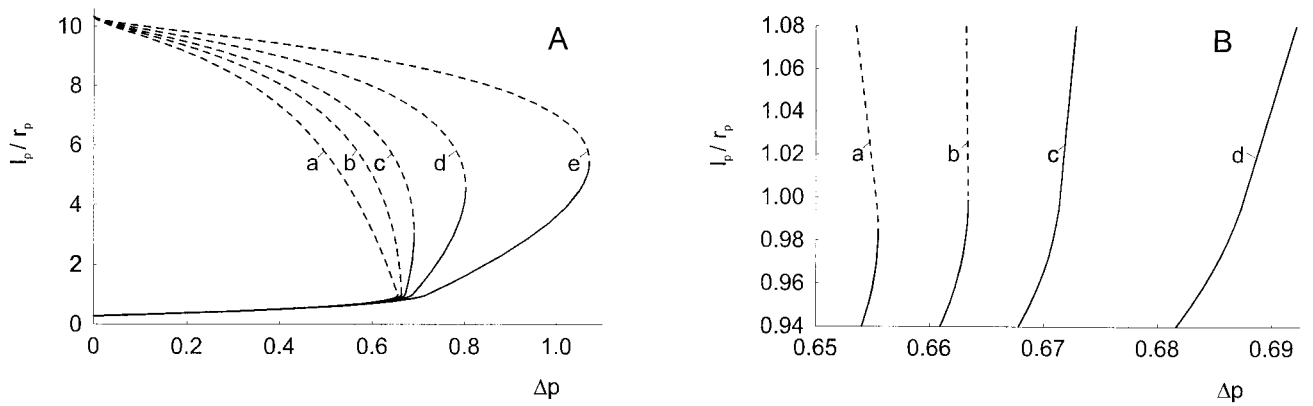

FIGURE 2 The ratio between the equilibrium projection length and the pipette radius as a function of the relative aspiration pressure for five different ratios K/γ and at the relative pipette radius $r_p = 0.5$. (*A*) For complete course of aspiration and (*B*) enlarged in the region where the critical projection length is close to the pipette radius, $l_p \approx r_p$. The values of the ratio are, (*a*) $K/\gamma = 0$, (*b*) 0.5, (*c*) 1, (*d*) 2, and (*e*) 4. The stable states and unstable states are represented by solid and dashed lines respectively. The point of the maximal equilibrium aspiration pressure is the critical point. The function $\Delta p(l_p)$ is smooth in the whole interval, but has a discontinuous second derivative in the point where the projection length becomes equal to the pipette radius. The relative unit of the aspiration pressure corresponds to 23 Pa.

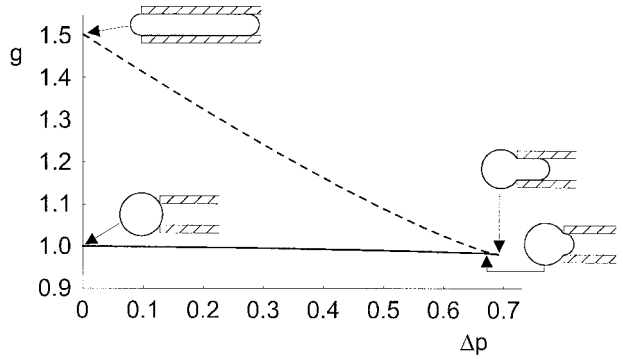

FIGURE 3 Thermodynamic potential g versus aspiration pressure Δp for the equilibrium states at the relative pipette radius $r_p = 0.5$ and the elasticity parameter $K/\gamma = 1$. The solid line represents the stable states and the dashed line the unstable ones. The level of the aspiration is indicated schematically at four characteristic points. The states aspirated beyond the critical point are in an unstable equilibrium and are on a higher thermodynamic potential than the stable equilibrium states.

Eq. 9), so the spontaneous transitions to the continuous flow regime at aspiration pressures less than the critical are not likely to occur.

Critical projection length

The position of the critical point can be determined by finding the maximal possible equilibrium aspiration pressure and the corresponding projection length. Because the analytical relations connecting the geometrical variables are complicated, we calculated the maximal equilibrium aspiration pressure numerically. The obtained predictions for the critical projection length as a function of the relative pipette radius at five ratios K/γ are presented in Fig. 4. In the case of a liquid droplet ($K/\gamma = 0$), the critical projection length is always a few percent smaller than the pipette radius (this result was already calculated by Drury and Dembo, 1999). However, if the droplet is elastic, $K/\gamma \neq 0$, the critical projection length increases significantly at small pipette radii.

This behavior can be explained. If the cortical tension is constant, as it is in the case of a liquid droplet, the equilibrium aspiration pressure is proportional directly to the difference of curvatures of the inner and the outer spherical part (a curvature is an inverse of a radius), $1/r_{in} - 1/r_{out}$ (Eq. 5). At the beginning of aspiration, the inner curvature ($1/r_{in}$) increases more rapidly with l_p than the outer one ($1/r_{out}$) and Δp increases ($d\Delta p/dl_p > 0$). When l_p is near r_p, however, Δp decreases ($d\Delta p/dl_p < 0$). That is because, when l_p is near r_p, the inner curvature smoothly approaches its final constant value $1/r_p$ and thus begins to increase more slowly with l_p than the outer one. It follows that the maximum equilibrium pressure—the critical pressure—is attained before l_p reaches r_p.

In the case of an elastic droplet, the cortical tension increases as the droplet area increases during aspiration. The greater cortical tension resists aspiration more strongly and the critical point of aspiration is only attained at larger projection lengths. Once the critical projection length becomes larger than the pipette radius, its dependence on the pipette radius (and also on the ratio K/γ) is much stronger. As a consequence of the two different regimes of the projection growth, the functions $l_{p(crit)}(r_p)$ have a discontinuous first derivative in the point where $l_{p(crit)} = r_p$. Note that the elasticity only weakly affects the smallest possible value of

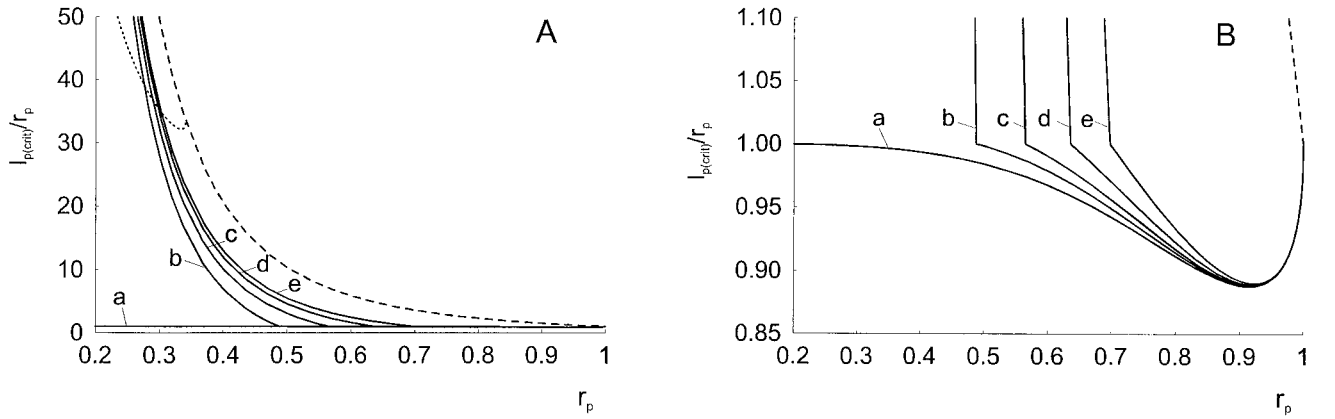

FIGURE 4 The ratio between the critical projection length and the pipette radius as a function of the relative pipette radius for five values of the elasticity parameter K/γ. Values of K/γ are the same as in Fig. 2. (*A*) Full scale and (*B*) enlarged in the region where the critical projection length is close to the pipette radius, $l_{p(crit)}/r_p \approx 1$. If $K/\gamma \neq 0$, the critical projection length at small pipette radii exceeds the pipette radius. The critical projection lengths are minimal around $r_p \approx 0.92$ for all five values of K/γ. The dashed line represents projection lengths of a fully aspirated droplet and thus presents the geometrical limit for critical projection lengths. The dotted line represents projection lengths when the droplet area is increased to two times the initial area of the spherical droplet and thus presents the approximate practical limit of aspiration when all the membrane bilayer is smoothed out (Evans and Yeung, 1989).

the critical projection lengths, which is around $r_p \approx 0.92$ for all reasonably expected values of the ratio K/γ (Fig. 4 *B*).

Whether the critical length exceeds or does not exceed the pipette radius depends both on the ratio K/γ and the relative pipette radius. The values on the boundary between the two cases are presented in Fig. 5. At smaller pipette radii, even a small K/γ has a significant effect on the elongation of the critical projection length. In contrast, if the relative pipette radius is larger than 0.9164, even extreme elasticity ($K/\gamma \rightarrow \infty$) cannot significantly affect the position of the critical point, and the critical projection length is always less than the pipette radius. In the case of $K/\gamma \sim 1$, which corresponds to the observed values of the parameter K/γ (Needham and Hochmuth, 1992), the critical projection length exceeds the pipette radius for the relative pipette radii under ~0.6. Therefore, the elongation of the critical projection lengths above the pipette radius could be detected experimentally.

The measurements of the position of the critical point should be carried out carefully. The reason for this is that the equilibrium projection lengths near the critical point can depend strongly on the aspiration pressure (for the case of the relative pipette radius $r_p = 0.5$ and $K/\gamma = 1$, see Fig. 2). Thus, considering the limited precision of the aspiration pressure set up in current experiments, it might be difficult to measure the exact value of the critical projection length at all relative pipette radii. In addition, the noninstantaneous response of the neutrophil to the change of the aspiration pressure should be considered. Therefore, to avoid missing the critical point, approaching toward the critical point through the equilibrium states by increasing the aspiration pressure should be performed slowly. Or, alternatively, the procedure described by Zhelev and Hochmuth (1994) can be used, in which the neutrophils were first driven in the continuous flow regime and then relaxed to the equilibrium by a decrease of the aspiration pressure.

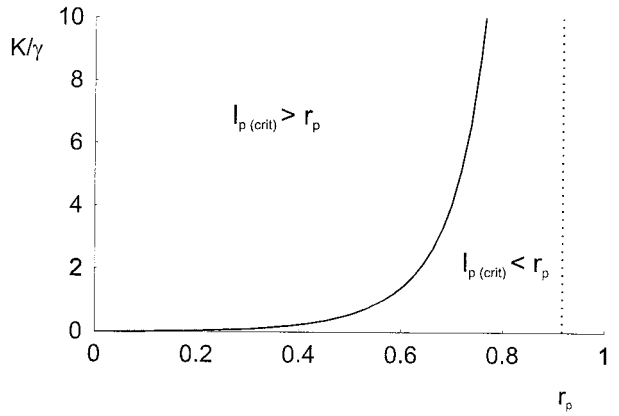

FIGURE 5 The limiting values of the ratio K/γ and r_p of the two regimes of behavior of the elastic droplet. At large pipette radii and small ratios K/γ the droplet behaves as a liquid droplet with the critical projection length slightly smaller than the pipette radius. At small pipette radii and high ratios K/γ, the critical projection lengths are larger than the pipette radius. The vertical dotted line represents the asymptotic value of $r_p \approx 0.9164$, beyond which the critical projection length is less than the pipette radius even in the limit $K/\gamma \rightarrow \infty$.

Critical aspiration pressure

The approximation (based on the basic liquid-drop model) that the critical point is reached when the projection length reaches the pipette radius, leads to the estimation that the critical pressure of aspiration is an inverse function of the pipette radius (Evans and Yeung, 1989). Our numerical calculation of the critical pressure as the function of the pipette radius for $K/\gamma = 0$ shows that this estimation is accurate to a few percent. Even for the pipette radius of 0.92, where the critical projection length deviates most from the pipette radius (Fig. 4 *B*), the difference is only about 15%. In the case of an elastic droplet, the critical pressure increases with K/γ, but the general inverse relation to the pipette radius is conserved (Fig. 6). However, it should be stressed once more that, when $K/\gamma \neq 0$ (*curves b*, *c*, *d*, and *e* in Fig. 6), the critical pressures can occur at larger projection lengths and can therefore not be directly compared to the existing experimental data, where the critical pressure was generally reported to be measured at $l_p = r_p$.

The imprecise definition of the critical aspiration pressure used in the literature should not affect the measurements of the cortical tension. That is because the law of Laplace, which is used as the relation between the aspiration pressure and the effective cortical tension, is valid in all the equilibrium states and not only at the critical point. So, if the law of Laplace is strictly used, the cortical tension can be safely determined by measuring any of the equilibrium aspiration pressures.

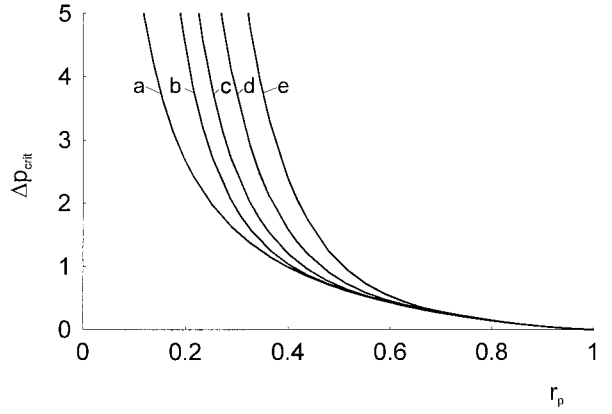

FIGURE 6 The relation between the relative critical pressure and the relative pipette radius for five values of the elasticity parameter K/γ. Values of K/γ are the same as in Fig. 2. The critical pressure increases with increasing K/γ.

CONCLUSION

In this paper, we theoretically analyzed the stability of the equilibrium states of micropipette aspiration with the aim to rigorously characterize the critical point of aspiration. Our analysis shows that the critical point of aspiration does not necessarily occur when the projection length in the pipette becomes equal to the pipette radius. Specifically, it shows that, if the neutrophil membrane-cortex complex has an elastic area expansivity, the neutrophil can be held in a static equilibrium even if its projection length in the pipette exceeds the pipette radius. This feature was, in fact, observed (see, for example, Fig. 4 in Evans and Yeung, 1989 or Fig. 9 in Zhelev and Hochmuth, 1994), but could not be described within the basic liquid-drop model of neutrophil rheology.

We emphasize that the notion "critical aspiration pressure" has to be used with caution. Because the critical pressure is defined as the largest possible aspiration pressure at which the neutrophil can be held in a static equilibrium, it should not be generally attributed to the aspiration pressure, which is attained when the projection length reaches the pipette radius. Nevertheless, the imprecise definition of the critical pressure should normally not affect the measurements of the effective cortical tension. As long as the law of Laplace is strictly used, the cortical tension can be reliably determined by the measurements of the equilibrium aspiration pressure.

Finally, we suggest that the presented analysis serves as a basis for further measurements of the neutrophil elastic properties. Although the exact positions of the critical point of aspiration at all relative pipette radii might be difficult to obtain, a comparison between the presented predictions and the measured critical projection length as a function of the relative pipette radius can yield new information on the values of the neutrophil area expansivity modulus K and the constant cortical tension γ.

If experiments reveal that the equilibrium neutrophil behavior differs significantly from the predictions of the presented analysis, the simple neutrophil elastic area expansion rigidity could not be the main neutrophil elastic property and at least two further options for the neutrophil elasticity should be investigated. The first possibility is that the neutrophil cytoplasm has significant elastic rigidity. The second possibility is that the cortical tension is not only a function of the area dilation, but depends also on the history of aspiration, i.e., the cortical tension is governed by some active processes that can be triggered by the applied stress.

APPENDIX A. MINIMIZATION OF THE THERMODYNAMIC POTENTIAL

In this appendix, we present a rigorous calculation of the equilibrium states of an aspirated droplet. The equilibrium states are obtained by the minimization of the system's thermodynamic potential. In the case of the model used in this paper, the result could be also derived from the force-balance equations. However, the energy minimization approach enables us to perform the stability analysis of the equilibrium states.

The equilibrium states of an aspirated droplet are the extrema of the thermodynamic potential defined in Eq. 11. Because of the fixed droplet volume constraint, the extrema of the thermodynamic potential correspond to the stationary points of the functional

$$g' = -\Delta p v_p + a + \frac{1}{2}\frac{K}{\gamma}(a-1)^2 + M(v - v_0), \quad \text{(A1)}$$

where M is the Lagrange multiplier for the volume and v_0 is the fixed overall volume of the droplet (in the relative units $v_0 = 1$).

In the stationary point, the variation of the functional with respect to shape is zero, $\delta g' = 0$. Written out, the variation of g' is

$$\delta g' = -\Delta p \delta v_p + \bar{\tau}\delta a + M(\delta v_p + \delta v_{out}), \quad \text{(A2)}$$

where $\bar{\tau}$ is the dimensionless effective cortical tension, $\bar{\tau} = \bar{T}/\gamma = 1 + (K/\gamma)(a - 1)$, and v_{out} is the relative volume of the part of the droplet outside the pipette. We used the relation $v = v_{out} + v_p$.

The aspirated droplet is axisymmetric, therefore we can parametrize the droplet shape in terms of its axisymmetric contour and express the functional in terms of an integral over this contour. We get a classical problem of the calculus of variations; the stationary shapes correspond to the solutions of the Euler–Lagrange equations derived for our system (for a general reference on the calculus of variations see Elsgolc (1961), and, for the calculus of variations applied to the calculation of equilibrium shapes of closed lipid membranes, see Jülicher and Seifert (1994) and Božič et al. (1997)).

The standard parameterization of a closed axisymmetric surface is done via coordinates $r(s)$, $z(s)$, and $\psi(s)$, where r is the radial distance of the contour to the axis of symmetry, z is the position along the axis, ψ is the contour angle, and s is the arclength along the contour (Fig. 7). The angle of the contour $\psi(s)$ is defined by the equation $\tan\psi = \mathrm{d}z/\mathrm{d}r$.

Using integral relations for the volume and area,

$$v_{out} = \frac{3}{4}\int_A^B r^2 \sin\psi \, \mathrm{d}s,$$

$$v_p = \frac{3}{4}\int_B^C r^2 \sin\psi \, \mathrm{d}s,$$

and

$$a = \frac{1}{2}\int_A^C r \, \mathrm{d}s,$$

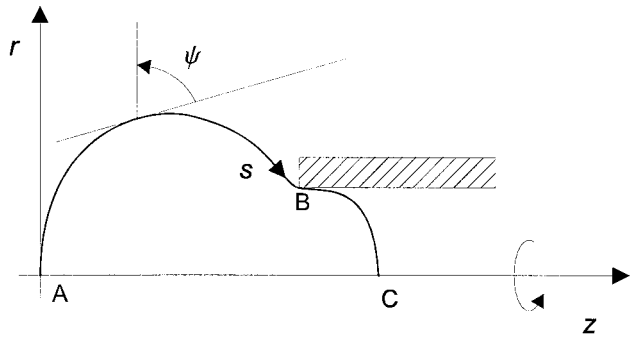

FIGURE 7 Cell contour during aspiration into a micropipette. The contour is parametrized by variables $r(s)$, $z(s)$, and $\psi(s)$, where s is the arclength along it.

we can express the variation of the functional g' as

$$\delta g' = \delta \int_A^B \mathcal{L}_{out} ds + \delta \int_B^C \mathcal{L}_{in} ds, \tag{A3}$$

where both Lagrangian functions can be written in a similar form,

$$\mathcal{L}_i = \tfrac{3}{4} r^2 M_i \sin\psi + \tfrac{1}{2}\bar{\tau} r + \Gamma_i(\dot{r} - \cos\psi) + F_i(\dot{z} - \sin\psi). \tag{A4}$$

The subscript i stands for "out" when referring to the part of the droplet outside the pipette, and for "in" when referring to the part of the droplet in the pipette. Note that $M_{out} = M$, whereas $M_{in} = M - \Delta p$. Note also that, for the sake of simplicity, the subscript is omitted from the variables r, ψ, and z. The additional Lagrange multipliers $\Gamma_i(s)$ and $F_i(s)$ had to be introduced because the variables $r(s)$, $z(s)$, and $\psi(s)$ are not independent but are related through equations $\dot{r} = dr/ds = \cos\psi$ and $\dot{z} = dz/ds = \sin\psi$.

The variational procedure can be carried out in a relatively simple way by using the Hamilton notation. We therefore define

1. The vector of variables $\mathbf{x}_i$, $\mathbf{x}_i = (r, \psi, z, \Gamma_i, F_i)$.
2. The vector of the generalized momentum $\mathbf{p}_i = \mathcal{L}_{i\dot{\mathbf{x}}_i}$,

$$\mathbf{p}_i = \left(\frac{\partial \mathcal{L}_i}{\partial \dot{r}}, \frac{\partial \mathcal{L}_i}{\partial \dot{\psi}}, \frac{\partial \mathcal{L}_i}{\partial \dot{z}}, \frac{\partial \mathcal{L}_i}{\partial \dot{\Gamma}_i}, \frac{\partial \mathcal{L}_i}{\partial \dot{F}_i}\right).$$

In our case, the generalized momentum $\mathbf{p}_i = (\Gamma_i, 0, F_i, 0, 0)$.

3. The Hamiltonian $H_i = -\mathcal{L}_i + \dot{\mathbf{x}}_i \cdot \mathbf{p}_i$. In our case, the Hamiltonian is

$$H_i = -\tfrac{3}{4} r^2 M_i \sin\psi - \tfrac{1}{2}\bar{\tau} r + \Gamma_i \cos\psi + F_i \sin\psi. \tag{A5}$$

The classic result of variational calculus is that the variation $\delta g'$ vanishes if the Euler–Lagrange equations,

$$\mathcal{L}_{i\mathbf{x}_i} - \frac{d}{ds}\mathbf{p}_i = 0, \tag{A6}$$

and the boundary conditions,

$$[\mathbf{p}_{out} \cdot \delta \mathbf{x}_{out} - H_{out}\delta s]_A^B + [\mathbf{p}_{in} \cdot \delta \mathbf{x}_{in} - H_{in}\delta s]_B^C = 0, \tag{A7}$$

are satisfied.

Thus, we obtain two sets of differential equations (one for i = in and the other for i = out) for the variables r, ψ, z, Γ_i, and F_i:

$$\tfrac{3}{2} r M_i \sin\psi + \tfrac{1}{2}\bar{\tau} = \dot{\Gamma}_i, \tag{A8}$$

$$\tfrac{3}{4} r^2 M_i \cos\psi + \Gamma_i \sin\psi - F_i \cos\psi = 0, \tag{A9}$$

$$\dot{F}_i = 0, \tag{A10}$$

$$\dot{r} = \cos\psi, \tag{A11}$$

$$\dot{z} = \sin\psi. \tag{A12}$$

Because the variations in points A, B, and C (Fig. 7) are independent, the boundary condition (Eq. A7) can be written in three separate parts. Written out, the conditions for boundary points A and C are

$$(\Gamma_{out}\delta r + F_{out}\delta z - H_{out}\delta s)\big|_A = 0$$

and

$$(\Gamma_{in}\delta r + F_{in}\delta z - H_{in}\delta s)\big|_C = 0, \tag{A13}$$

whereas the condition in junction point B reads

$$(\Delta\Gamma\delta r + \Delta F\delta z - \Delta H\delta s)\big|_B = 0, \tag{A14}$$

where $\Delta\Gamma = \Gamma_{out} - \Gamma_{in}$, $\Delta F = F_{out} - F_{in}$ and $\Delta H = H_{out} - H_{in}$.

The variations δr, δz, and δs are independent, so each term in Eqs. A13 and A14 has to vanish separately. In points A and C, the variations δz and δs are arbitrary, therefore F_i and H_i at those points have to be zero. In contrast, the radius is fixed in points A and C, $\delta r = 0$, so at those points, the boundary condition gives no constraints on Γ_i. Similarly, because r and z in the junction are fixed (by the fixed coordinates of the pipette tip), $\delta r|_B = 0$ and $\delta z|_B = 0$, it follows that the boundary condition gives no constraints on $\Delta\Gamma$ and ΔF. The variation δs, however, is arbitrary and therefore $\Delta H = 0$.

Because the Lagrangian $\mathcal{L}_i$ does not explicitly depend on s, the Hamiltonian has to be constant along each integration contour. The same is true for F_i (Eq. A10), therefore,

$$H_{out} = 0 \quad \text{and} \quad H_{in} = 0, \tag{A15}$$

$$F_{out} = 0 \quad \text{and} \quad F_{in} = 0. \tag{A16}$$

In summary, the equilibrium neutrophil shape should satisfy Eqs. A8–A12 and A15–A16.

By expressing the spherical parts with $r = r_i \sin\psi$, one can easily verify that the spherical shapes are the equilibrium shapes. The law of Laplace (Eq. 5) can be derived by eliminating Γ_i from Eqs. A9 and A5, and then writing them in the spherical parameterization,

$$\text{Inside:} \quad \frac{3}{2}(M - \Delta p) + \frac{\bar{\tau}}{r_{in}} = 0, \tag{A17}$$

$$\text{Outside:} \quad \frac{3}{2}M + \frac{\bar{\tau}}{r_{out}} = 0. \tag{A18}$$

The law of Laplace (Eq. 5) is just the difference of these two equations written out in the normal, nondimensionless, form.

When the part in the pipette becomes a hemisphere with the radius of the pipette, it starts to elongate as a cylinder. Analogous with the analysis presented above, it can be shown that this elongated shape is also in equilibrium. First, one has to divide the contour into three parts, the two spherical parts and a cylinder in between. Instead of two sets of Euler–Lagrange equations (Eqs. A8–A12), one obtains three sets, one for each part. The two spherical parts still solve these equations and the same can be easily verified for the cylinder by expressing the cylinder contour with $r = r_p$ ($\psi = \pi/2$).

The boundary condition in this case is

$$[\mathbf{p}_{out} \cdot \delta \mathbf{x}_{out} - H_{out}\delta s]_A^{B_1} + [\mathbf{p}_{cyl} \cdot \delta \mathbf{x}_{cyl} - H_{cyl}\delta s]_{B_1}^{B_2} + [\mathbf{p}_{in} \cdot \delta \mathbf{x}_{in} - H_{in}\delta s]_{B_2}^{C} = 0, \tag{A19}$$

where the subscript cyl stands for the variables in the cylindrical part, and B_1 and B_2 are the junction points between the spherical parts and the cylindrical one (Fig. 8). Now, the boundary condition (Eq. A19) can be written in four distinct parts, the conditions for points A and C and the conditions for the two junction points B_1 and B_2. Because of the cylindrical geometry, the variations of s and z in points B_1 and B_2 are not independent

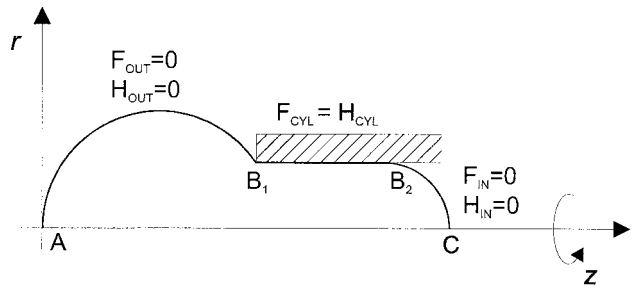

FIGURE 8 The representation of the aspirated droplet in the case when $l_p > r_p$. The values of the Hamiltonian H_i and the Lagrange multiplier F_i are indicated.

$(z|_{B_2} - z|_{B_1} = s|_{B_2} - s|_{B_1})$ and the boundary condition in the two junction points cannot be written in three distinct terms. Therefore, the boundary condition at the junctions yields $(F_{cyl} - F_{out} + H_{out} - H_{cyl})|_{B_1} = 0$ and $(F_{in} - F_{cyl} + H_{cyl} - H_{in})|_{B_2} = 0$. Because for the spherical parts F_i and H_i are zero, we have $H_{cyl} = F_{cyl}$. This relation and the definition of H_{cyl} give the value of the Lagrange multiplier M_{in},

$$M_{in} = M - \Delta p = -\frac{2}{3}\frac{\bar{\tau}}{r_p}. \tag{A20}$$

Because of this relation, Eq. A17 can be fulfilled only if $r_{in} = r_p$. Therefore, in the presence of the cylindrical part, the spherical part in the pipette has to be exactly a hemisphere with the radius r_p.

APPENDIX B. STABILITY CONDITION

In this appendix, we present the derivation of the stability condition (Eq. 12) in terms of observable quantities Δp and l_p (Eq. 13). Choosing l_p as the only independent variable, the equilibrium and stability conditions can be expressed as $dg/dl_p = 0$ and $d^2g/dl_p^2 > 0$. Written out, the derivatives read,

$$\frac{dg}{dl_p} = -\Delta p \frac{dv_p}{dl_p} + \frac{dw}{dl_p}, \tag{B1}$$

$$\frac{d^2g}{dl_p^2} = -\Delta p \frac{d^2v_p}{dl_p^2} + \frac{d^2w}{dl_p^2}. \tag{B2}$$

Because of the equilibrium condition, the aspiration pressure can be written as

$$\Delta p = \frac{dw/dl_p}{dv_p/dl_p}. \tag{B3}$$

After the differentiation of Δp with respect to l_p and by expressing dw/dl_p in terms of Δp (Eq. B3) and d^2w/dl_p^2 in terms of d^2g/dl_p^2 (Eq. B2) one obtains

$$\frac{d\Delta p}{dl_p} = \frac{d^2g/dl_p^2}{dv_p/dl_p}. \tag{B4}$$

Because dv_p/dl_p is positive, the condition of stability of the aspirated droplet can be rewritten as

$$\frac{d\Delta p}{dl_p} > 0. \tag{B5}$$

REFERENCES

Bessis, M. 1973. Living Blood Cells and Their Ultrastructure. Springer-Verlag, Berlin.

Božič, B., S. Svetina, and B. Žekš. 1997. Theoretical analysis of the formation of membrane microtubes on axially strained vesicles. *Phys. Rev. E.* 55:5834–5842.

Dong, C., and R. Skalak. 1992. Leukocyte deformability: finite element modeling of large viscoelastic deformation. *J. Theor. Biol.* 158:173–193.

Drury, J. L., and M. Dembo. 1999. Hydrodynamics of micropipette aspiration. *Biophys. J.* 76:110–128.

Elsgolc, L. E. 1961. Calculus of Variations. Pergamon Press, Oxford.

Evans, E., and B. Kukan. 1984. Passive material behavior of granulocytes based on large deformation and recovery after deformation tests. *Blood.* 64:1028–1035.

Evans, E., and A. Yeung. 1989. Apparent viscosity and cortical tension of blood granulocytes determined by micropipet aspiration. *Biophys. J.* 56:151–160.

Jülicher, F., and U. Seifert. 1994. Shape equations for axisymmetric vesicles: a clarification. *Phys. Rev. E.* 49:4728–4731.

Needham, D., and R. M. Hochmuth. 1992. A sensitive measure of surface stress in the resting neutrophil. *Biophys. J.* 61:1664–1670.

Schmid-Schönbein, G. W., Y. Y. Shih, and S. Chien. 1980. Morphometry of human leukocytes. *Blood.* 56:866–875.

Schmid-Schönbein, G. W., K.-L. P. Sung, H. Tözeren, R. Skalak, and S. Chien. 1981. Passive mechanical properties of human leukocytes. *Biophys. J.* 36:243–256.

Sheterline, P., and J. E. Rickard. 1989. The cortical actin filament network of neutrophil leucocytes during phagocytosis and chemotaxis. *In* The Neutrophil: Cellular Biochemistry and Physiology. M. B. Hallett, editor. CRC Press, Boca Raton, FL. 141–165.

Svetina, S., B. Božič, and B. Žekš. 1998. A mechanism for the establishment of polar cell morphology based on the cytoskeleton-derived forces exerted on the cell boundary. *Eur. Biophys. J.* 28:74–77.

Ting-Beall, H. P., D. Needham, and R. M. Hochmuth. 1993. Volume and osmotic properties of human neutrophils. *Blood.* 81:2774–2780.

Tsai, M. A., R. S. Frank, and R. E. Waugh. 1994. Passive mechanical behavior of human neutrophils: effect of cytochalasin B. *Biophys. J.* 66:2166–2172.

Tsai, M. A., R. E. Waugh, and P. C. Keng. 1998. Passive mechanical behavior of human neutrophils: effects of colchicine and paclitaxel. *Biophys. J.* 74:3282–3291.

Yeung, A., and E. Evans. 1989. Cortical shell–liquid core model for passive flow of liquid-like spherical cells into micropipets. *Biophys. J.* 56:139–149.

Zhelev, D. V., and R. M. Hochmuth. 1994. Human neutrophils under mechanical stress. *In* Cell Mechanics and Cellular Engineering. V. C. Mow, F. Guilak, R. Tran-Son-Tay, and R. M. Hochmuth, editors. Springer-Verlag, New York. 3–21.

Zhelev, D. V., D. Needham, and R. M. Hochmuth. 1994. Role of the membrane cortex in neutrophil deformation in small pipets. *Biophys. J.* 67:696–705.